Porphyrin−Dithienothiophene π-Conjugated Copolymers: Synthesis and Their Applications in Field-Effect Transistors and Solar Cells

Xuebin Huang,[†,‡] Chunli Zhu,[†,‡] Shiming Zhang,[†,§] Weiwei Li,[†,§] Yunlong Guo,[†,§] Xiaowei Zhan,*[,†] Yunqi Liu,*[,†] and Zhishan Bo*[,†]

Beijing National Laboratory for Molecular Sciences and Institute of Chemistry, Chinese Academy of Sciences, Beijing 100190, China, Department of Chemistry, Beijing Institute of Technology, Beijing 100083, China, and Graduate School, Chinese Academy of Sciences, Beijing 100039, China

Received June 24, 2008; Revised Manuscript Received August 4, 2008

ABSTRACT: Soluble conjugated alternating porphyrin−dithienothiophene copolymers—single-bond linked (**I**) and triple-bond linked (**IIa** and **IIb**)—were synthesized by palladium(0)-catalyzed Stille and Sonagashira coupling reactions, respectively. The thermal, electrochemical, optical, charge transport, and photovoltaic properties of these copolymers were examined; the effect of the triple bond was studied. **I** exhibits onset decomposition temperature (T_d) of 410 °C and glass-transition temperature (T_g) of 180 °C, higher than those of **IIb** (T_d, 330 °C; T_g, 130 °C). The absorption spectrum of **I** in thin film exhibits a sharp Soret band at 450 nm and two weak Q-bands at 563−619 nm, while **IIb** exhibits a sharp Soret band at 491 nm and a strong Q-band at 760 nm. The emission maxima of **I** and **IIb** in solution are located at 642 and 722 nm respectively. **IIb** is electrochemically active in both the oxidation and reduction regions, while **I** shows only oxidation peak. The field-effect hole mobilities as high as 2.1×10^{-4} cm^2 V^{-1} s^{-1} were obtained for these copolymers. Polymer solar cells (PSCs) were fabricated based on the blend of the polymers and methanofullerene [6,6]-phenyl C61-butyric acid methyl ester (PCBM). The power conversion efficiency (PCE) of 0.3% was achieved under AM 1.5, 100 mW/cm^2 for the PSC using **IIb**:PCBM (1:3, w/w) as active layer. The PCE of the PSC based on **IIb**:PCBM (1:3, w/w) is double that based on **I**:PCBM (1:2, w/w), consistent with that **IIb** exhibits stronger Q-band absorption and higher mobility at room temperature.

Introduction

Porphyrin molecules have been intensively studied over many years since they are involved in light-harvesting, charge generation, and other biological or biochemical processes.[1] In recent years, porphyrin molecules and polymers have attracted attention as useful materials for organic photonics and electronics since they possess large planar π-conjugated structure, unique electronic properties, and good photochemical and thermal stability. Porphyrin derivatives exhibit large third-order nonlinear optical response, strong two-photon absorption, and potential application in photodynamic therapy.[2] Moreover, applications of porphyrin molecules and polymers in organic electronic devices such as light-emitting diodes (OLEDs), field-effect transistors (OFETs), and solar cells have been reported. Recently, we reported a series of star-shaped oligomers and polymers and hyperbranched polymers based on porphyrin as efficient red light-emitting materials.[3] OFET devices made using porphyrin small molecules exhibit carrier mobilities up to 0.2 cm^2 V^{-1} s^{-1}.[4] However, there have been few reports in which porphyrin polymers were used in OFETs as active layers. The device performance based on the porphyrin polymers is quite poor. For example, OFETs made using a porphyrin−diacetylene polymer give mobilities of 1×10^{-7} cm^2 V^{-1} s^{-1} at room temperature and 2×10^{-6} cm^2 V^{-1} s^{-1} at 175 °C.[5] Organic solar cells using porphyrin-containing small molecules, oligomers, and polymers as active layers give low power conversion efficiencies (PCE).[6] For example, the efficiency of the device based on porphyrin triad, porphyrin-containing oligomers, main-chain porphyrin polymers, and porphyrin-grafted poly(phenylene vinylene) is 0.035%,[6a] 0.0081%,[6b] 1−10 ppm,[6c] and 0.33%,[6d] respectively. The main reason for the low PCEs is limited light absorption of porphyrin. The absorption spectra of porphyrin unit exhibit narrow and strong Soret band (410−430 nm), weak Q-bands (530−540 nm), and blank between the Soret and Q bands.

Current trends in device fabrication favor solution-processing. In general, polymers are more suitable for solution processing than small molecules to obtain good-quality thin films. Some side-chain[7] and nonconjugated main-chain porphyrin polymers[8] have been reported. Their electronic and optical properties have not changed much in comparison with that of porphyrin small molecules because there is no direct π-conjugation between neighboring units. In order to improve the properties of the porphyrin polymers, main-chain conjugated porphyrin polymers have been synthesized.[9] However, if the porphyrin units are directly connected, steric hindrance between them disturbs formation of an extended conjugation. Some efforts have been devoted to synthesis of porphyrin polymers with improved solubility and conjugation. Main-chain conjugated porphyrin polymers with various spacers including arylene, aryleneethynylene and phenylenevinylene between porphyrins have been synthesized, but very few electronic device results have been reported.[10]

The planarity and S···S interaction of fused thiophenes have been found to promote highly ordered π-stacked structures and high hole mobilities. Several groups have reported synthesis of fused thiophene derivatives and applications in OFETs.[11] Recently, we fabricated high-performance OFET devices using the fused thiophene molecules which we synthesized.[12]

In this paper, we present the synthesis of soluble main-chain π-conjugated porphyrin−dithienothiophene copolymers (Figure 1). Introduction of dithienothiophene (DTT) and diethynyldithienothiophene into the porphyrin polymer main chain can reduce steric hindrance, extend conjugation, enhance absorption, and improve charge transport property. 3,4,5-Tris(dodecyloxy)-phenyl groups at positions 10 and 20 of the zinc porphyrin ring

* Corresponding authors. E-mail: xwzhan@iccas.ac.cn, liuyq@iccas.ac.cn, zsbo@iccas.ac.cn.
[†] Institute of Chemistry, Chinese Academy of Sciences.
[‡] Beijing Institute of Technology.
[§] Graduate School, Chinese Academy of Sciences.

10.1021/ma801407u CCC: $40.75
Published on Web 09/11/2008

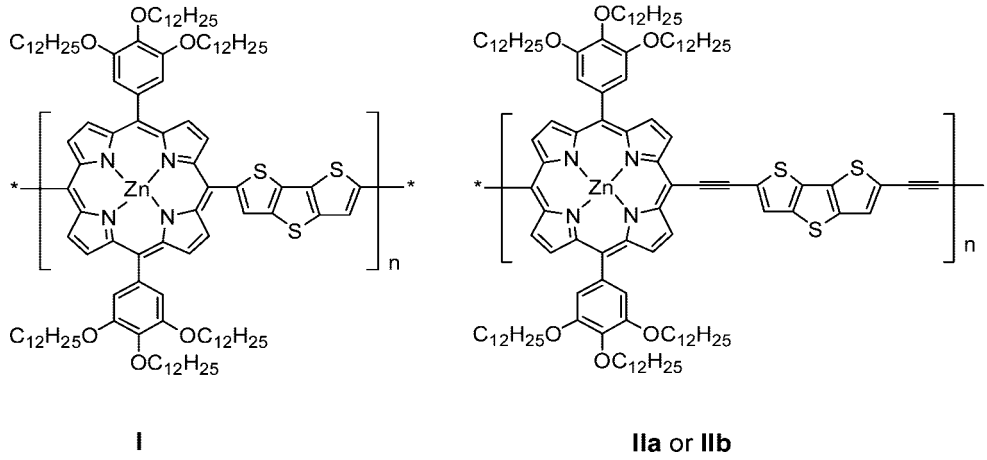

Figure 1. Chemical structures of the porphyrin−dithienothiophene copolymers.

Scheme 1. Synthesis of Porphyrin Monomers

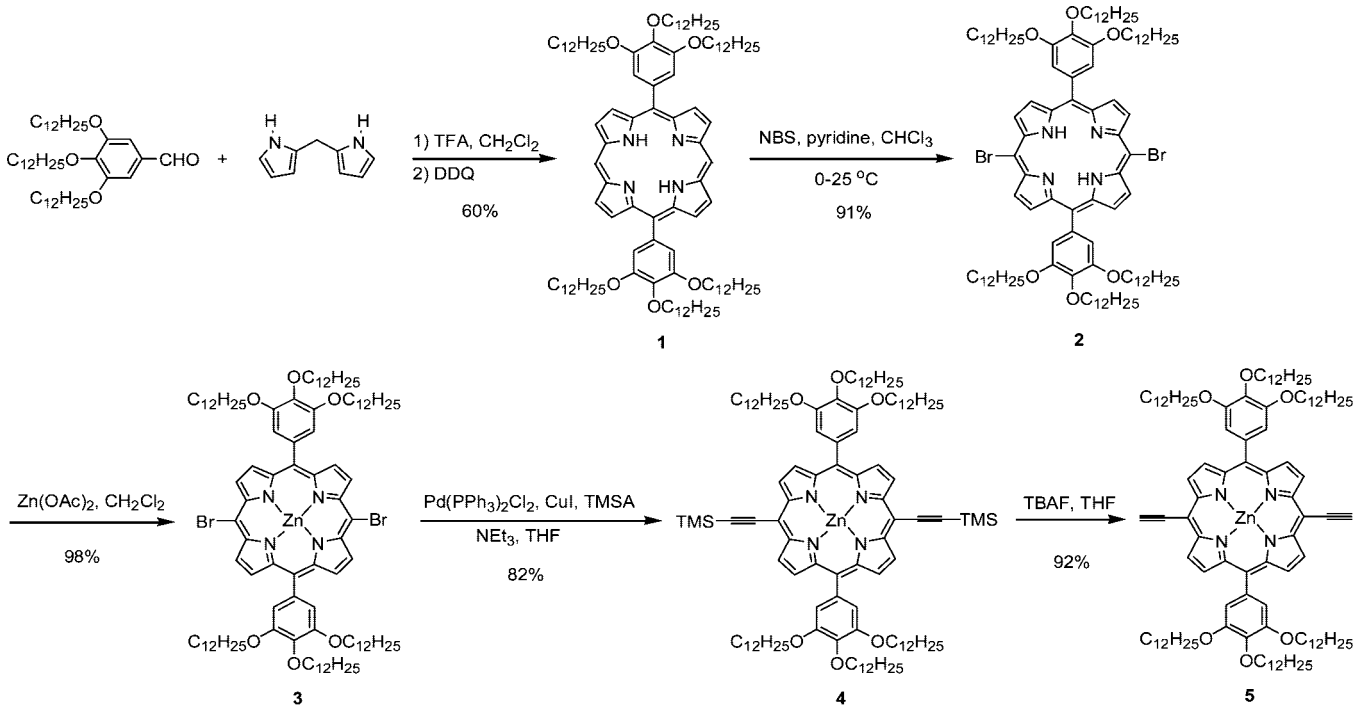

can improve solubility, induce self-assembly, and enhance molecular ordering. In addition, the polymers were used in organic field-effect transistors and solar cells to demonstrate their potential utility.

Results and Discussion

Synthesis and Characterization. The synthesis of the porphyrin monomers is shown in Scheme 1. New intermediate *trans*-substituted porphyrin **1** was synthesized in 60% yield by acid-catalyzed condensation of dipyrromethane with 3,4,5-tridodecyloxybenzaldehyde, followed by oxidation with 2,3-dichloro-5,6-dicyano-1,4-benzoquinone (DDQ) at room temperature, similar to Lindsey's method.[13] After bromination reaction with NBS and then coordination reaction with zinc acetate, zinc dibromoporphyrin **3** was readily obtained in high yield. Another monomer diethynylporphyrin **5** was synthesized in high yield from zinc dibromoporphyrin **3** by Sonogashira coupling with trimethylsilylacetylene (TMSA), followed by removal of the protecting groups with tetrabutylammonium fluoride (TBAF). All new compounds have been characterized by ^{1}H NMR, ^{13}C NMR, MS and elemental analysis. The data are consistent with the proposed structures.

Scheme 2 shows the synthesis of the porphyrin polymers as well as the small molecule reference. The reference compound **0** was synthesized in high yield by coordination reaction of porphyrin **1** with zinc acetate. The single-bond linked porphyrin−DTT copolymer (**I**) was synthesized by Stille coupling reaction between dibromoporphyrin **3** and DTT ditin. Two different strategies were employed to synthesize triple-bond linked porphyrin−DTT polymer (**IIa** and **IIb**). As shown in Scheme 2, different monomers were employed for the polycondensation based on Sonogashira coupling reaction. The monomers are zinc dibromoporpyrin **3** and diethynyl dithienothiophene in route a, while they are zinc diethynylporphyrin **5** and dibromodithienothiophene in route b. Polymers **IIa** and **IIb** are obtained through these two routes, respectively.

All these polymers have good solubility in common organic solvents such as chloroform, THF, and toluene. All the polymers can be readily processed to form smooth and pinhole-free films upon spin-coating. The 3,4,5-tris(dodecyloxy)phenyl groups at

Scheme 2. Synthesis of Porphyrin Polymers and Small Molecule

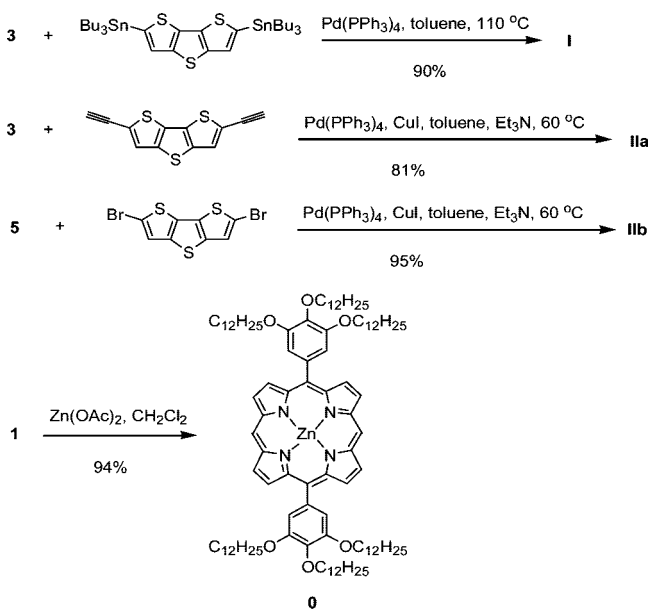

Table 1. Molecular Weights of the Polymers[a]

	M_n	M_w	PDI
I	46 500	97 800	2.1
IIa	12 700	25 800	2.0
IIb	15 300	26 900	1.8

[a] Number average molecular weight (M_n), weight average molecular weight (M_w) and polydispersity index (PDI) determined by means of GPC with THF as eluent on the basis of polystyrene calibration.

positions 10 and 20 of the zinc porphyrin ring of the polymers play an important role in solubilizing.

Molecular weights of the polymers were determined by gel permeation chromatography (GPC) using polystyrene standards as calibrants (Table 1). Polymer **I** has a M_n of 46 500, corresponding to a degree of polymerization of *ca.* 25. Polymers **IIa** and **IIb** show M_n values of 12 700 and 15 300, corresponding to degrees of polymerization of *ca.* 7 and 8, respectively. The single-bond linked porphyrin−DTT copolymer **I** has a much higher M_n value than the triple-bond linked porphyrin−DTT polymers **IIa** and **IIb**; **IIb** has a higher M_n than **IIa**. This is probably related to a side reaction involving the ethynyl groups. Under the same reaction conditions of Sonogashira coupling, oxidative coupling of ethynyl groups usually occurs as a side reaction to give a butadiyne.[14] Diethynylporphyrin undergoes oxidative coupling with more difficulty than diethynyldithienothiophene due to the increased steric hindrance between larger porphyrin units. This butadiyne byproduct will reduce the amount of the ethynyl group to react with bromo segments. Furthermore, the butadiyne byproduct of diethynyldithienothiophene has a low solubility and prevents the polymer chain growth in reaction system. In comparison with **IIa**, **IIb** exhibits higher molecular weight, better elemental analysis, and red-shifted absorption, suggesting that the second route is more preferable. A similar phenomenon was found by Krebs et al. in synthesis of zinc porphyrin linked poly(phenyleneethynylene).[15]

The thermal properties of the polymers were determined by thermogravimetric analysis (TGA) and differential scanning calorimetry (DSC) under nitrogen. Polymers **I** and **IIb** have good thermal stability with onset decomposition temperatures of 410 and 330 °C, respectively (Figure 2). Figure 3 shows DSC traces of polymers **I** and **IIb**. While the polymer samples were heated, glass transitions were observed at 180 (**I**) and 130 °C

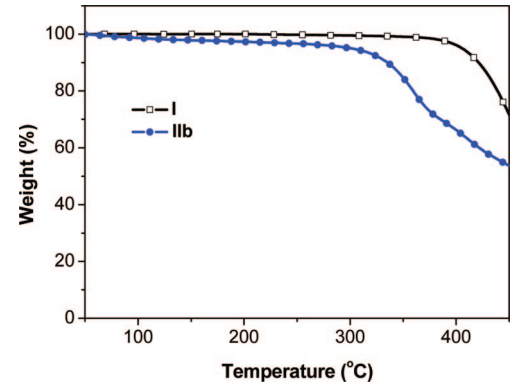

Figure 2. TGA curves of polymers **I** and **IIb**.

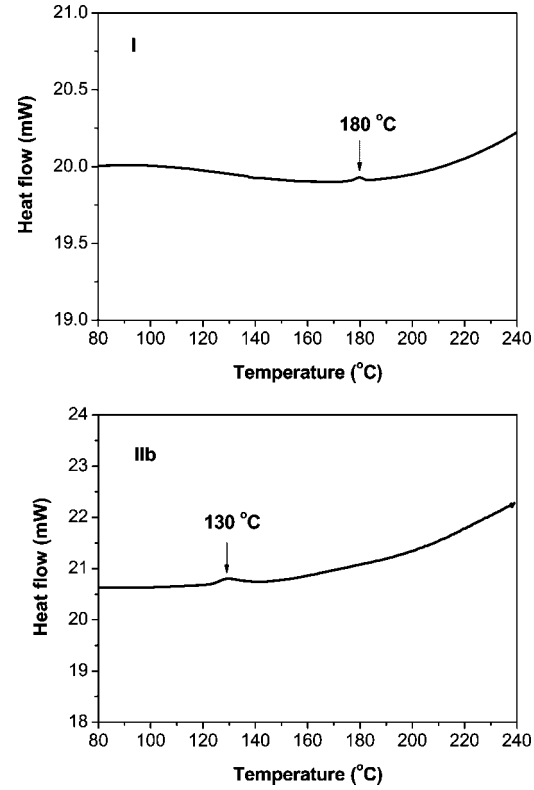

Figure 3. DSC curves of polymers **I** and **IIb**.

(**IIb**), but no melting point, suggesting that the polymers are amorphous. The higher decomposition temperature and higher glass-transition temperature of **I** are probably related to its higher molecular weight.

Absorption and Fluorescence Spectra. Figure 4 shows the UV−vis absorption spectra of the porphyrin polymers as well as the porphyrin small molecule in solution. The small molecule reference shows a sharp Soret band at 412 nm and a Q-band at 538 nm, which is a typical absorption profile for porphyrin compounds. All the polymers show absorptions in the regions of Soret band and Q-band. Compared to the reference absorption, the Soret band and Q-band of the polymers are broadened. In comparison with that for the small molecule reference **0**, the absorption spectrum of the single-bond linked porphyrin−DTT polymer **I** exhibits a red shift of *ca.* 24 nm, caused by the larger conjugation of the polymer. The Soret band and Q-band of the triple-bond linked porphyrin−DTT polymer **IIa** further red shift *ca.* 28 and 94 nm, respectively; the Q-bands are broadened and stronger, compared to that for the single-bond linked counterpart **I**. A similar phenomenon was observed in porphyrin−thiophene polymers.[10a] In polymer **I**, steric hindrance between directly

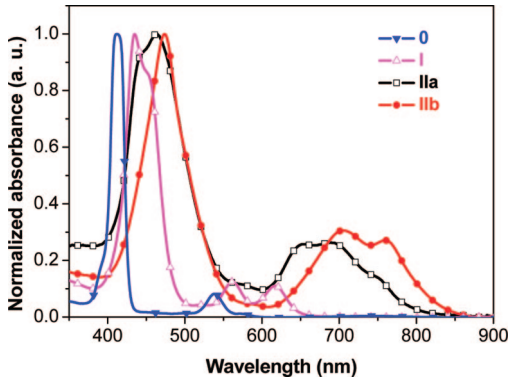

Figure 4. UV−vis absorption spectra of the porphyrin polymers as well as the reference in chloroform.

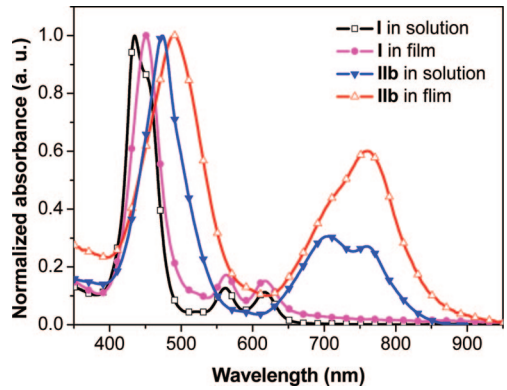

Figure 5. UV−vis absorption spectra of the porphyrin polymers in thin film.

linked porphyrin and DTT units leads to twisted main chain and limited conjugation; while in polymer **IIa**, the triple-bond linker between porphyrin and DTT units reduces the steric hindrance and, therefore, promotes coplanarity and extended π-conjugation. Interestingly, the Soret band and Q-band of the triple-bond linked porphyrin-DTT polymer **IIb**, synthesized by route b, exhibit red shift of 10 and 47 nm respectively, compared to **IIa**, synthesized by route a. This result is consistent with the GPC measurements which show that **IIb** possesses a higher molecular weight than **IIa** does.

The UV−vis spectra of polymer **I** and **IIb** in thin film are shown in Figure 5. The absorption spectrum of polymer **I** in thin film is similar to that in solution, which is probably related to the twisted main chain. However, the Soret band and Q-band of **IIb** are broadened and red shift 18 and 57 nm respectively, compared to that in solution. It is worth noting that the Q-band of **IIb** in thin film is located at 650−850 nm and is much stronger than that in solution. This is beneficial to sunlight harvesting because the solar emission spectrum is peaked at 600−800 nm. The red-shifted absorption and stronger Q-band of **IIb** in thin film is probably related to the aggregation caused by more coplanar main chain.

Figure 6 shows photoluminescence (PL) spectra of the porphyrin polymers as well as the reference in solution. The single-bond linked porphyrin−DTT polymer **I** exhibits an emission peaked at 643 nm, 10 nm red-shifted compared to the small molecule reference **0**. The emission spectra of the triple-bond linked porphyrin−DTT polymers **IIa** and **IIb** red shift 81 nm compared to the single-bond linked porphyrin−DTT polymer **I**. It is in accord with their UV−vis data. Since internal conversion is rapid, the fluorescence peaks of the polymers seem to occur at the onset positions of their absorption Q-bands, similar to that of the porphyrin−thiophene polymers.[10a] The

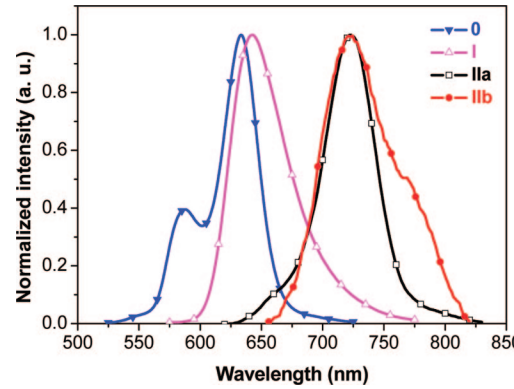

Figure 6. PL spectra of the porphyrin polymers as well as the reference compound in chloroform.

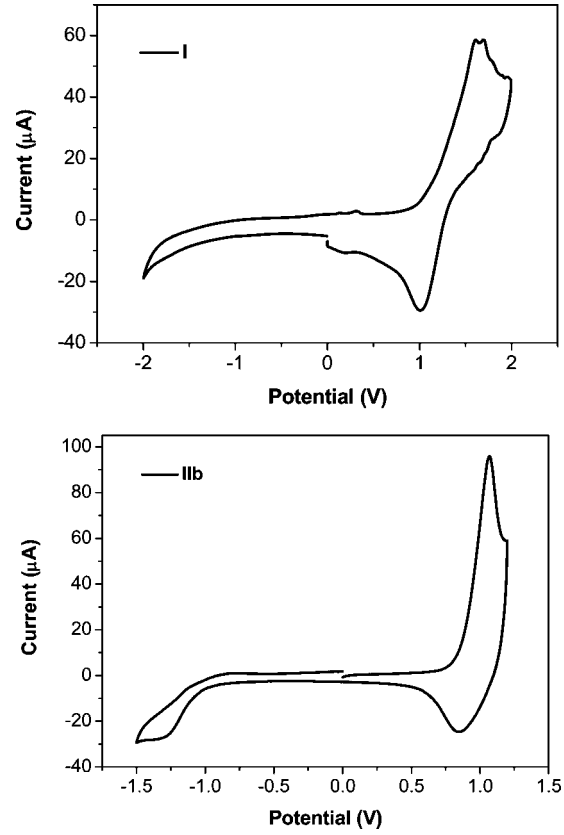

Figure 7. Cyclic voltammograms for **I** (top) and **IIb** (bottom) in CH_3CN/0.1 M $[^nBu_4N]^+[PF_6]^-$ at 50 mV/s. The horizontal scale refers to an anodized Ag wire pseudo-reference electrode.

fluorescence of all these polymers in thin films upon excitation at Soret or Q-band maxima was hardly observed presumably due to aggregation-induced PL quenching and/or some self-absorption due to overlap between absorption Q-bands and PL spectra.

Electrochemistry

Cyclic voltammograms of the polymers are illustrated in Figure 7. **I** shows only one quasi-reversible oxidation peak, while **IIb** shows both one quasi-reversible oxidation peak and one irreversible reduction peak, due to the presence of electron deficient triple bond group. The former has an onset oxidation potential at 1.08 V vs Ag^+/Ag; the latter has an onset oxidation potential at 0.86 V vs Ag^+/Ag and an onset reduction potential at −1.06 V vs Ag^+/Ag. The HOMO and LUMO values of **I** are estimated at −5.5 and −3.6 eV respectively from the onset

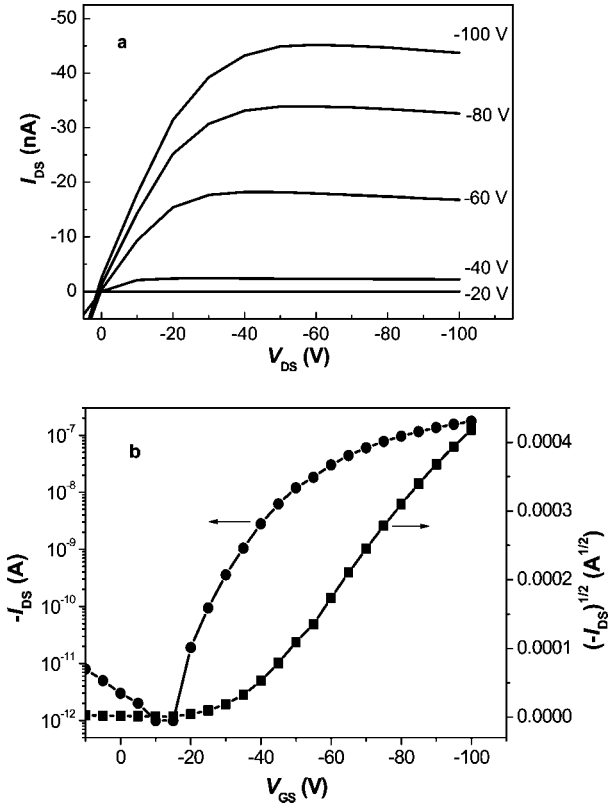

Figure 8. (a) Current−voltage characteristics (I_{DS} vs V_{DS}) at different gate voltages (V_{GS}), and (b) $-I_{DS}$ and $(-I_{DS})^{1/2}$ vs V_{GS} plots at V_{DS} of −100 V for a top contact device (annealing at 175 °C, $W = 3$ mm, $L = 50$ μm, 100 nm of **I**).

Table 2. The Performance of OFETs Based on I and IIb before and after Annealing

polymer	condition	mobility (cm^2 V^{-1} s^{-1})	on/off ratio	threshold voltage (V)
I	no annealing	5.0×10^{-5}	4×10^4	−11
	annealing at 175 °C	2.1×10^{-4}	2×10^5	−36
IIb	no annealing	1.1×10^{-4}	2×10^3	−3.3
	annealing at 80 °C	5.4×10^{-5}	1×10^3	−1.4

oxidation potential and the optical band gap estimated from onset absorption edge, assuming the absolute energy level of $FeCp_2^{+/0}$ to be 4.8 eV below vacuum.[16] From the onset oxidation and reduction potentials, the HOMO and LUMO levels of **IIb** are estimated as −5.2 and −3.3 eV respectively.

Field-Effect Transistors. OFET devices were fabricated in a top-contact configuration using Au as source and drain electrodes to study charge transport properties of these polymers. The mobility of devices in the saturation regime was extracted by

$$I_{DS} = (W/2L)C_i\mu(V_{GS} - V_{th})^2 \quad (1)$$

where I_{DS} is the drain current, μ is the field-effect mobility, L and W are the channel length and width respectively, C_i is the insulator capacitance per unit area, and V_{GS} and V_{th} are the gate voltage and threshold voltage respectively.

Both **I** and **IIb** perform as p-type semiconductors. Figure 8 shows the drain current (I_{DS}) versus drain-source voltage (V_{DS}) characteristics and transfer characteristics ($-I_{DS}$ vs V_{GS} plotted on a logarithmic scale and $(-I_{DS})^{1/2}$ vs V_{GS}, at $V_{DS} = -100$ V) of the transistors based on **I** with thermal annealing at 175 °C. The output curve shows good saturation behavior with clear saturation currents. Table 2 summarizes the performance of OFETs based on **I** and **IIb** before and after annealing. Interestingly, the device performance of the two polymers shows different trends with thermal annealing. The OFET based on **I** exhibits a mobility of 5.0×10^{-5} cm^2 V^{-1} s^{-1} with current on/off ratio of 4×10^4 at room temperature; the thermal annealing at 175 °C leads to improved performance with a mobility of 2.1×10^{-4} cm^2 V^{-1} s^{-1} and current on/off ratio of 2×10^5. The OFET based on **IIb** exhibits a mobility of 1.1×10^{-4} cm^2 V^{-1} s^{-1} with current on/off ratio of 2×10^3 and a low threshold voltage of ca. −3.3 V at room temperature; the thermal annealing at 80 °C leads to decreased performance with a mobility of 5.4×10^{-5} cm^2 V^{-1} s^{-1} and current on/off ratio of 1×10^3. **IIb** shows higher mobility than **I** at room temperature, probably because it has more coplanar and extended π-conjugated main chain and stronger aggregation and intermolecular interaction in thin film, as suggested by UV data of thin films.

To understand the effect of thermal annealing on the device performance, we employed X-ray diffraction (XRD) and atomic force microscopy (AFM) to gain insight into the thin film morphology. The XRD patterns for thin films of **I** and **IIb** before and after annealing (see Supporting Information Figure S1) show only very broad peaks, typical for amorphous materials. This result is consistent with high T_gs of the polymers (Figure 3). From AFM images (Figure S2 in Supporting Information), no crystalline domains were observed for all the thin films, consistent with the XRD and DSC results. However, the thermal annealing does exert somewhat impact on the thin film morphology. Some defects were observed from the film of **I** at room temperature, while the film becomes more uniform and smooth with lower defect density after annealing at 175 °C. The film of **IIb** before annealing is more uniform and smooth than that after annealing at 80 °C. The FET device performance is strongly related to the film morphology and quality; the charge transport is influenced by the defect density which could trap a large amount of charge carriers. Thus, thermal annealing leads to different film quality and therefore, different device performance.

Photovoltaic Cells. In the fabrication of bulk heterojunction photovoltaic cells, methanofullerene [6,6]-phenyl C61-butyric acid methyl ester (PCBM) is a typical electron acceptor. To investigate the potential of these porphyrin−dithienothiophene copolymers for photovoltaic applications, we used **I** or **IIb** as an electron donor and PCBM as an electron acceptor, and fabricated bulk heterojunction PSCs with a structure of ITO/PEDOT:PSS/blend/Al. Both estimated LUMO and HOMO levels of the donor **I** or **IIb** are more than 0.5 eV higher than that of the acceptor PCBM, indicating that the energy level positions of the donor and acceptor are suitable for efficient charge transfer and separation at the interface between the donor and acceptor.[17] Photoluminescence (PL) quenching in donor/acceptor composites is a symptom of efficient photoinduced charge transfer between the donor and acceptor.[18] To get insight into the possible photoinduced electron transfer from the polymers to PCBM, PL spectroscopy of the polymers in the presence of PCBM was carried out. PL of the blend of **I**/PCBM (1:2, w/w) and **IIb**/PCBM (1:3, w/w) was hardly observed upon excitation at Soret or Q-band maxima of the polymers, similar to that of neat **I** and **IIb**. Thus, PL spectra of the blend cannot give clear evidence for photoinduced electron transfer from the polymers to PCBM.

The PSCs were fabricated using the blends with different weight ratios of **I** or **IIb** to PCBM. The current density (J) versus voltage (V) curve of the PSC with the structure ITO/PEDOT:PSS/**IIb**:PCBM (1:3, w/w)/Al under illumination of simulated AM 1.5 at 100 mW/cm^2 is shown in Figure 9 as an example. The open circuit voltage (V_{oc}), short circuit current density (J_{sc}), fill factor (FF), and the power conversion efficiency (PCE) of

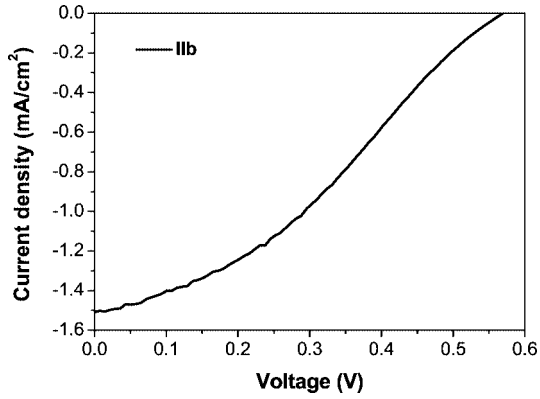

Figure 9. Current density−voltage characteristics of a device with the structure ITO/PEDOT:PSS/**IIb**:PCBM (1:3, w/w)/Al under the illumination of an AM 1.5 solar simulator, 100 mW/cm^2.

Table 3. Photovoltaic Performance of the PSCs

polymer	polymer/PCBM (w/w)	V_{oc} (V)	J_{sc} (mA/cm^2)	FF	PCE (%)
I	1:1	0.23	0.12	0.33	0.01
	1:2	0.46	1.29	0.26	0.15
	1:3	0.45	0.45	0.29	0.06
	1:4	0.52	0.62	0.29	0.09
IIb	1:1	0.53	0.88	0.33	0.15
	1:2	0.52	1.25	0.35	0.23
	1:3	0.58	1.52	0.34	0.30
	1:4	0.59	1.17	0.30	0.21

the devices are summarized in Table 3. When **IIb**:PCBM weight ratio is 1:3, the PSC device exhibited the best performance; V_{oc}, J_{sc}, FF and PCE reached 0.58 V, 1.52 mA/cm^2, 0.34 and 0.3%, respectively. The PCE of 0.3% is among the highest for the PSCs based on porphyrin-containing molecules and polymers.[6] Optimization of the device structures and thermal annealing can be expected to substantially increase the PCE of the PSCs. The PCE of 0.3% achieved for the PSC using **IIb**:PCBM (1:3, w/w) as active layer is double that using **I**:PCBM (1:2, w/w) as active layer, consistent with **IIb**'s exhibiting stronger absorption at Q-band and higher mobility at room temperature.

Conclusion

Soluble conjugated alternating porphyrin−dithienothiophene copolymers were synthesized by palladium(0)-catalyzed Stille or Sonagashira coupling reactions. The triple bond exerts significant influence on the thermal, electrochemical, optical, charge transport, and photovoltaic properties of these copolymers. The single-bond linked polymer possesses higher molecular weight and better thermal stability than the triple-bond linked counterpart. In comparison with the single-bond linked polymer **I**, the triple-bond linked polymers **IIa** and **IIb** exhibit red-shifted absorption and emission spectra, especially significantly red-shifted and much stronger Q-band absorption, since **IIa** and **IIb** have coplanar and extended π-conjugated main chain related to the triple bond spacer. The triple-bond linked polymer **IIb** is electrochemically active in both the oxidation and reduction regions, while the single-bond linked polymer **I** shows only an oxidation peak. The field-effect hole mobilities up to 2.1×10^{-4} cm^2 V^{-1} s^{-1} were obtained for these porphyrin−dithienothiophene copolymers. **IIb** shows higher mobility than **I** at room temperature, probably because it has more coplanar and extended π-conjugated main chain and stronger aggregation and intermolecular interaction in thin film. The device performance of the two polymers shows different trends with thermal annealing; thermal annealing leads to different film quality and therefore, different device performance. The PCE of 0.3% was achieved for the PSC using **IIb**:PCBM (1:3, w/w) as active layer, among the highest reported for the PSCs based on porphyrin-containing molecules and polymers. The PCE of the PSC based on **IIb**:PCBM (1:3, w/w) is double that based on **I**:PCBM (1:2, w/w), consistent with that **IIb** exhibits stronger Q-band absorption and higher mobility at room temperature.

Experimental Section

Materials. 3,4,5-Tris(dodecyloxy)benzaldehyde,[19] dipyrromethane,[20] 2,6-dibromo-dithieno[3,2-*b*:2′,3′-*d*]thiophene,[21] 2,6-bis(tri-*n*-butylstannyl)dithieno[3,2-*b*:2′,3′-*d*]thiophene,[22] and 2,6-diethynyldithieno[3,2-*b*:2′,3′-*d*]thiophene[23] were synthesized according to literature methods. THF and toluene were distilled from sodium−benzophenone under nitrogen prior to use. Triethylamine was distilled from CaH_2 under nitrogen prior to use. All other reagents were used as received.

Characterization. The ^{1}H and ^{13}C NMR spectra were measured on a Bruker AVANCE 400 MHz spectrometer using tetramethylsilane ($\delta = 0$ ppm) as an internal standard. Mass spectra were measured on a GCT-MS micromass (U.K.) spectrometer using the electron impact (EI) mode or on a Bruker Daltonics BIFLEX III MALDI-TOF Analyzer using MALDI mode. Elemental analyses were carried out using a FLASH EA1112 elemental analyzer. Solution (chloroform) and thin-film (on quartz substrate) UV−vis absorption spectra were recorded on a JASCO V-570 spectrophotometer. Solution (chloroform) and thin-film (on quartz substrate) emission spectra were collected on a Hitachi F-4500 spectrofluorophotometer. Electrochemical measurements were carried out under nitrogen on a deoxygenated solution of tetra-*n*-butylammonium hexafluorophosphate (0.1 M) in acetonitrile using a computer-controlled Zahner IM6e electrochemical workstation, a glassy-carbon working electrode coated with polymer films, a platinum-wire auxiliary electrode, and an Ag wire anodized with AgCl as a pseudoreference electrode. Potentials were referenced to the ferrocenium/ferrocene ($FeCp_2^{+/0}$) couple by using ferrocene as an internal standard. Thermogravimetric analysis (TGA) measurements were performed on Shimadzu thermogravimetric analyzer (model DTG-60) under a nitrogen flow at a heating rate of 10 °C/min. DSC measurements were performed using a Perkin-Elmer differential scanning calorimeter (DSC7) under N_2 at a heating rate of 20 °C min^{-1}. The gel permeation chromatography (GPC) measurements were performed on a Waters 515 chromatograph connected to a Waters 2414 refractive index detector, using THF as eluent and polystyrene standards as calibrants. Three Waters Styragel columns (HT2, 3, 4) connected in series were used.

Fabrication and Characterization of Field-Effect Transistors. FET devices were fabricated with a top-contact configuration. A heavily doped n-type Si wafer with a SiO_2 layer of 500 nm and a capacitance of 7.5 nF/cm^2 was used as the gate. Octadecyltrichlorosilane (OTS) was used as a self-assembled surface modifier for SiO_2. A 110 nm thick (±10 nm) semiconductor film was spin-coated on top of the OTS-treated SiO_2 from 10 mg/mL *o*-dichlorobenzene solution of **I** or **IIb**. Gold source and drain contacts (50 nm) were deposited on the organic layer through a shadow mask under high vacuum. The channel length (L) and width (W) were 50 μm and 3 mm, respectively. All measurement of electric properties was carried out at ambient conditions and room temperature using a Keithley 4200 SCS semiconductor parameter analyzer. Device annealing was carried out at 175 °C (**I**) or 80 °C (**IIb**) for 1 h inside a vacuum oven at 0.1 Pa.

Fabrication and Characterization of Polymer Solar Cells. The PSCs were fabricated in the traditional sandwich structure. Poly(3,4-ethylene dioxythiophene)−poly(styrene sulfonate) (PEDOT:PSS) was spin-coated from an aqueous solution (Bayer AG) on a precleaned indium tin oxide (ITO)/glass substrate, and was dried subsequently at 140 °C in vacuum oven for 20 min, giving a thickness of *ca.* 30 nm as measured by Ambios Technology XP-2 surface profilometer. The photosensitive blend layers were prepared by spin-coating an *o*-dichlorobenzene solution containing both **I** or **IIb** and PCBM with the total concentration of 20 mg/mL on the

ITO/PEDOT:PSS electrode, followed by drying at 80 °C for 30 min. The thickness of the active layer is about 60 nm. Finally, the cathode consisting of 120 nm of aluminum was thermally deposited on the top of polymer film at 1×10^{-4} Pa. The active area of one cell was 4 mm^2. These experiments were carried out in a nitrogen-filled glovebox. The current−voltage ($I-V$) measurements of the devices were conducted on a computer-controlled Keithley 236 Source Measure Unit. A xenon lamp with AM 1.5 filter was used as the white light source, and the optical power on the sample was 100 mW/cm^2.

5,15-Bis(3,4,5-tris(dodecyloxy)phenyl)porphyrin (1). A solution of 3,4,5-tris(dodecyloxy)benzaldehyde (900 mg, 1.37 mmol) and dipyrromethane (200 mg, 1.37 mmol) in CH_2Cl_2 (140 mL) was purged with nitrogen for 30 min, and then trifluoroacetic acid (TFA) (100 mg, 0.87 mmol) was added. The mixture was stirred for 3 h at room temperature, and then DDQ (620 mg, 2.7 mmol) was added. After the mixture was stirred at room temperature for an additional 15 min, the reaction was quenched by adding triethylamine (1 mL). The solvent was removed, and the residue was purified by flash column chromatography on silica gel using dichloromethane as the eluent. Recrystallization from diethyl ether/methanol gave a purple solid (640 mg, 60%). ^{1}H NMR (400 MHz, $CDCl_3$): δ 10.30 (s, 2H), 9.39 (d, $J = 4.6$ Hz, 4H), 9.18 (d, $J = 4.6$ Hz, 4H), 7.48 (s, 4H), 4.32 (t, $J = 6.5$ Hz, 4H), 4.14 (t, $J = 6.4$ Hz, 8H), 1.99 (m, 4H), 1.89 (m, 8H), 1.68 (m, 4H), 1.49 (m, 8H), 1.31 (m, 96H), 0.88 (m, 18H), −3.12 (s, 2H). ^{13}C NMR (100 MHz, $CDCl_3$): δ 151.50, 147.21, 145.20, 138.04, 136.30, 131.50, 131.09, 119.25, 114.51, 105.20, 73.79, 69.37, 32.00, 31.91, 30.64, 29.91, 29.86, 29.79, 29.70, 29.65, 29.53, 29.48, 29.47, 29.35, 26.36, 26.17, 22.75, 22.68, 14.16, 14.11. MS (MALDI): m/z 1568 (MH^+). Anal. Calcd for $C_{104}H_{166}N_4O_6$: C, 79.64; H, 10.67; N, 3.57. Found: C, 79.47; H, 10.70; N, 3.79%.

5,15-Dibromo-10,20-bis(3,4,5-tris(dodecyloxy)phenyl)porphyrin (2). Porphyrin **1** (300 mg, 0.19 mmol) was dissolved in chloroform (40 mL), and pyridine (0.2 mL) was added. The reaction mixture was cooled to 0 °C; NBS (66 mg, 0.38 mmol) was added. After stirring for 0.5 h, the mixture was allowed to warm up to room temperature and then stirred for 4 h. The reaction was quenched by addition of acetone (5 mL). The solvents were removed, and the residue was recrystallized from diethyl ether/methanol to afford a purple solid (300 mg, 91%). ^{1}H NMR (400 MHz, $CDCl_3$): δ 9.56 (d, $J = 4.2$ Hz, 4H), 8.95 (d, $J = 3.1$ Hz, 4H), 7.38 (s, 4 H), 4.33 (t, $J = 6.2$ Hz, 4H), 4.10 (t, $J = 6.1$ Hz, 8H), 2.00 (m, 4H), 1.86 (m, 8H), 1.70 (m, 4H), 1.45 (m, 8H), 1.32 (m, 96H), 0.88 (m, 18 H), −2.74 (s, 2 H). ^{13}C NMR (100 MHz, $CDCl_3$): δ 151.32, 138.27, 136.30, 121.55, 114.45, 103.67, 73.80, 69.38, 32.01, 31.92, 30.66, 29.91, 29.88, 29.80, 29.70, 29.65, 29.48, 29.36, 26.37, 26.16, 22.76, 22.68, 14.16, 14.10. MS (MALDI): m/z 1725 ($MH2^+$). Anal. Calcd for $C_{104}H_{164}Br_2N_4O_6$: C, 72.36; H, 9.58; N, 3.25. Found: C, 72.21; H, 9.36; N, 3.35%.

5,15-Dibromo-10,20-bis(3,4,5-tris(dodecyloxy)phenyl)porphyrin Zinc (3). To a solution of compound **2** (300 mg, 0.17 mmol) in dichloromethane (50 mL) was added a solution of $Zn(OAc)_2 \cdot H_2O$ (75 mg, 0.37 mmol) in methanol (3 mL). The reaction mixture was stirred at room temperature for 5 h. Evaporation of the solvent and purification by column chromatography (silica gel, CH_2Cl_2/petroleum ether (1/1)) afforded a purple solid (300 mg, 98%). ^{1}H NMR (400 MHz, $CDCl_3$): δ 9.73 (d, $J = 4.7$ Hz, 4H), 9.04 (d, $J = 4.7$ Hz, 4H), 7.30 (s, 4H), 4.18 (m, 4H), 4.06 (m, 8H), 1.91 (m, 4H), 1.81 (m, 8H), 1.63 (m, 4H), 1.44 (m, 8H), 1.31 (m, 96H), 0.86 (m, 18 H). ^{13}C NMR (100 MHz, $CDCl_3$): δ 150.90, 150.68, 150.20, 137.58, 136.86, 133.62, 133.07, 122.30, 114.41, 105.23, 73.54, 69.20, 32.00, 31.91, 30.40, 29.86, 29.79, 29.69, 29.62, 29.47, 29.42, 29.36, 26.22, 26.02, 22.75, 22.68, 14.15, 14.10. MS (MALDI): m/z 1786 (MH^+). Anal. Calcd for $C_{104}H_{162}Br_2N_4O_6Zn$: C, 69.80; H, 9.12; N, 3.13. Found: C, 70.05; H, 9.11; N, 3.21%.

5,15-Bis(trimethylsilylethynyl)-10,20-bis(3,4,5-tris(dodecyloxy)-phenyl)porphyrin Zinc (4). 3 (360 mg, 0.2 mmol) was dissolved in THF (10 mL) and triethylamine (5 mL) was added. The mixture was purged with nitrogen for 30 min. Then $Pd(PPh_3)_2Cl_2$ (7 mg, 0.01 mmol), CuI (2 mg, 0.01 mmol), and trimethylsilylacetylene (80 mg, 0.8 mmol) were added. After stirring at room temperature for 3 days under nitrogen, the solvent was removed under reduced pressure. The residue was purified by column chromatography (silica gel, CH_2Cl_2/petroleum ether (1/1)) to afford a green solid (301 mg, 82%). ^{1}H NMR (400 MHz, $CDCl_3$): δ 9.70 (d, $J = 4.6$ Hz, 4H), 9.03 (d, $J = 4.6$ Hz, 4H), 7.38 (s, 4H), 4.30 (t, $J = 6.4$ Hz, 4H), 4.11 (t, $J = 6.3$ Hz, 8H), 1.97 (m, 4H), 1.87 (m, 8H), 1.67 (m, 4H), 1.49 (m, 8H), 1.31 (m, 96H), 0.86 (m, 18H), 0.61 (s, 18H). ^{13}C NMR (100 MHz, $CDCl_3$): δ 152.36, 150.53, 150.23, 137.08, 136.81, 132.80, 131.06, 122.58, 114.12, 107.87, 101.51, 101.35, 73.32, 68.94, 32.03, 31.95, 30.16, 29.89, 29.81, 29.72, 29.69, 29.62, 29.51, 29.40, 29.21, 26.12, 25.98, 22.78, 22.61, 14.18, 14.13, 0.44. MS (MALDI): m/z 1822 (MH^+). Anal. Calcd for $C_{114}H_{180}N_4O_6Si_2Zn$: C, 75.06; H, 9.95; N, 3.07. Found: C, 75.07; H, 9.96; N, 3.14%.

5,15-Diethynyl-10,20-bis(3,4,5-tris(dodecyloxy)phenyl)porphyrin Zinc (5). Tetrabutylammonium fluoride (0.33 mL, 1 M in THF) was added to a stirred solution of porphyrin **4** (298 mg, 0.16 mmol) in THF (10 mL). After stirring for 5 min, water was added to quench the reaction. The solution was extracted with chloroform, washed with water and dried over anhydrous $MgSO_4$. After evaporation of the solvent, the residue was purified by column chromatography (silica gel, CH_2Cl_2/petroleum ether (1/1)) to give a green solid (252 mg, 92%). ^{1}H NMR (400 MHz, $CDCl_3$): δ 9.74 (d, $J = 4.6$ Hz, 4H), 9.07 (d, $J = 4.6$ Hz, 4H), 7.39 (s, 4H), 4.32 (t, $J = 6.4$ Hz, 4H), 4.19 (s, 2H), 4.12 (t, $J = 6.4$ Hz, 8H), 1.98 (m, 4H), 1.89 (m, 8H), 1.68 (m, 4H), 1.51 (m, 8H), 1.31 (m, 96H), 0.88 (m, 18 H). ^{13}C NMR (100 MHz, $CDCl_3$): δ 152.12, 150.64, 150.19, 137.34, 136.72, 132.80, 130.90, 122.40, 114.01, 99.77, 85.70, 83.66, 73.36, 68.98, 31.80, 31.71, 30.23, 29.66, 29.58, 29.55, 29.49, 29.45, 29.42, 29.27, 29.23, 29.15, 26.04, 25.84, 22.55, 22.47, 13.96, 13.90. MS (MALDI): m/z 1677 (M^+). Anal. Calcd for $C_{108}H_{164}N_4O_6Zn$: C, 77.22; H, 9.84; N, 3.34. Found: C, 77.31; H, 9.94; N, 3.45%.

5,15-Bis(3,4,5-tris(dodecyloxy)phenyl)porphyrin Zinc (0). To a solution of compound **1** (266 mg, 0.17 mmol) in dichloromethane (50 mL) was added a solution of $Zn(OAc)_2 \cdot H_2O$ (75 mg, 0.37 mmol) in methanol (3 mL). The reaction mixture was stirred at room temperature for 5 h. Evaporation of the solvent and purification by column chromatography (silica gel, CH_2Cl_2/petroleum ether (1/1)) afforded a purple-red solid (260 mg, 94%). ^{1}H NMR (400 MHz, $CDCl_3$): δ 10.33 (s, 2H), 9.45 (d, $J = 4.4$ Hz, 4H), 9.26 (d, $J = 4.4$ Hz, 4H), 7.48 (s, 4H), 4.33 (t, $J = 6.4$ Hz, 4H), 4.12 (t, $J = 6.4$ Hz, 8H), 2.00 (m, 4H), 1.90 (m, 8H), 1.70 (m, 4H), 1.52 (m, 8H), 1.31 (m, 96H), 0.88 (m, 18H). ^{13}C NMR (100 MHz, $CDCl_3$): δ 150.74, 149.90, 149.25, 137.47, 137.30, 132.32, 131.35, 119.90, 114.29, 105.92, 73.41, 69.01, 31.83, 31.74, 29.74, 29.70, 29.62, 29.51, 29.47, 29.44, 29.30, 29.26, 29.23, 29.18, 25.91, 22.58, 22.50, 13.98, 13.92. MS (MALDI): m/z 1631 ($MH2^+$). Anal. Calcd for $C_{104}H_{164}N_4O_6Zn$: C, 76.55; H, 10.13; N, 3.43. Found: C, 76.17; H, 10.07; N, 3.50%.

Poly{[10,20-bis(3,4,5-tris(dodecyloxy)phenyl)porphyrin zinc-5,15-diyl]-*alt*-(dithieno[3,2-*b*:2′,3′-*d*]thiophene-2,6-diyl)} (I). To a 50 mL round-bottom flask were added 5,15-dibromo-10,20-bis(3,4,5-tris(dodecyloxy)phenyl)porphyrin zinc **(3)** (357 mg, 0.2 mmol), 2,6-bis(tri-*n*-butylstannyl)dithieno[3,2-*b*:2′,3′-*d*]thiophene (155 mg, 0.2 mmol), and anhydrous toluene (10 mL). The mixture was deoxygenated with N_2 for 30 min. $Pd(PPh_3)_4$ (23 mg, 0.02 mmol) was added. After stirring at 110 °C for 3 days, the mixture was cooled to room temperature, and then KF (2.7 g in 5 mL water) was added and stirred for 2 h to remove the tin impurity. The mixture was extracted with chloroform and washed with water. The solution was concentrated to 15 mL and then dropped into 100 mL of methanol. The precipitate was filtered and washed with methanol. The solid was redissolved in 10 mL of chloroform and then dropped into 100 mL of acetone. The precipitate was filtered, and Soxhlet extracted with methanol for 2 days. Finally, the polymer was purified by size exclusion column chromatography over Bio-Rad Bio-Beads S-X1 eluting with THF to afford a greenish black solid (330 mg, 90%). ^{1}H NMR (400 MHz, $CDCl_3$): δ 9.47 (m, 4H), 9.19 (m, 4H), 8.33 (m, 2H), 7.47 (m, 4H), 4.35−4.14 (m,

12H), 2.05−0.82 (br, 138H). Anal. Calcd for $(C_{112}H_{164}N_4O_6S_3Zn)_n$: C, 73.75; H, 9.06; N, 3.07. Found: C, 71.78; H, 8.91; N, 3.13%. M_w, 97 800; M_w/M_n, 2.1.

Poly{[5,15-diethynyl-10,20-bis(3,4,5-tris(dodecyloxy)phenyl)porphyrin zinc]-*alt*-(dithieno[3,2-*b*:2′,3′-*d*]thiophene-2,6-diyl)}. Route a (IIa). To a 50 mL round-bottom flask were added 5,15-dibromo-10,20-bis(3,4,5-tris(dodecyloxy)phenyl)porphyrin zinc (**3**) (357 mg, 0.2 mmol), 2,6-diethynyl-dithieno[3,2-*b*:2′,3′-*d*]thiophene (49 mg, 0.2 mmol), anhydrous toluene (10 mL), and triethylamine (5 mL). The mixture was deoxygenated with N_2 for 30 min. $Pd(PPh_3)_4$ (3.5 mg, 0.003 mmol) and CuI (8 mg, 0.04 mmol) were added. The mixture was stirred at room temperature for 1 day and at 60 °C for 2 days. After cooling to room temperature, to the reaction mixture was added chloroform (50 mL) and filtered. The solution was concentrated and dropped into methanol (100 mL). After filtration, the polymer was purified by size exclusion column chromatography over Bio-Rad Bio-Beads S-X1 eluting with THF to afford a purplish black solid (300 mg, 81%). ^{1}H NMR (400 MHz, $CDCl_3$): δ 9.70 (br, 4H), 9.10 (br, 4H), 8.20 (br, 2H), 7.52 (m, 4H), 4.50−4.13 (br, 12H), 2.12−0.83 (br, 138H). Anal. Calcd for $(C_{116}H_{164}N_4O_6S_3Zn)_n$: C, 74.42; H, 8.83; N, 2.99. Found: C, 68.05; H, 8.42; N, 2.49%. M_w, 25 800; M_w/M_n, 2.0.

Route b (IIb). To a 50 mL round-bottom flask were added 5,15-diethynyl-10,20-bis(3,4,5- tris(dodecyloxy)phenyl)porphyrin zinc **(5)** (335 mg, 0.2 mmol), 2,6-dibromo-dithieno[3,2-*b*:2′,3′-*d*]thiophene (71 mg, 0.2 mmol), anhydrous toluene (10 mL), and triethylamine (5 mL). The mixture was deoxygenated with N_2 for 30 min. $Pd(PPh_3)_4$ (3.5 mg, 0.003 mmol) and CuI (8 mg, 0.04 mmol) were added. The mixture was stirred at room temperature for 1 day and at 60 °C for 2 days. After cooling to room temperature, to the reaction mixture was added chloroform (50 mL) and filtered. The solution was concentrated and dropped into methanol (100 mL). After filtration, the polymer was purified by size exclusion column chromatography over Bio-Rad Bio-Beads S-X1 eluting with THF to afford a purplish black solid (352 mg, 95%). ^{1}H NMR (400 MHz, $CDCl_3$): δ 9.70 (br, 4H), 9.10 (br, 4H), 8.20 (br, 2H), 7.50 (m, 4H), 4.53−4.01 (br, 12H), 2.10−0.80 (br, 138H). Anal. Calcd for $(C_{116}H_{164}N_4O_6S_3Zn)_n$: C, 74.42; H, 8.83; N, 2.99. Found: C, 70.22; H, 8.72; N, 3.00%. M_w, 26 900; M_w/M_n, 1.8.

Acknowledgment. This work was supported by the NSFC (Grants 20774104, 20721061, 20702004, 60736004, and 50673093), the MOST (Grants 2006AA03Z220 and 2006CB932100), and the Chinese Academy of Sciences (Grant KJCX2-YW-H12 and Hundred Talents Program). We thank Mr. Cheng Zhang for GPC measurements.

Supporting Information Available: XRD patterns and AFM images of thin films of **I** and **IIb** on OTS-treated SiO_2/Si substrate before and after annealing. This material is available free of charge via the Internet at http://pubs.acs.org.

References and Notes

(1) (a) Balaban, T. S. *Acc. Chem. Res.* **2005**, *38*, 612–623. (b) Imahori, H. *J. Phys. Chem. B* **2004**, *108*, 6130–6143.
(2) (a) Anderson, H. L.; Martin, S. J.; Bradley, D. D. C. *Angew. Chem., Int. Ed. Engl.* **1994**, *33*, 655–657. (b) Rath, H.; Sankar, J.; PrabhuRaja, V.; Chandrashekar, T. K.; Nag, A.; Goswami, D. *J. Am. Chem. Soc.* **2005**, *127*, 11608–11609. (c) Drobizhev, M.; Stepanenko, Y.; Rebane, A.; Wilson, C. J.; Screen, T. E. O.; Anderson, H. L. *J. Am. Chem. Soc.* **2006**, *128*, 12432–12433. (d) MacDonald, I. J.; Dougherty, T. J. *J. Porphyrins Phthalocyanines* **2001**, *5*, 105–129.
(3) (a) Li, B. S.; Li, J.; Fu, Y. Q.; Bo, Z. S. *J. Am. Chem. Soc.* **2004**, *126*, 3430–3431. (b) Fei, Z. P.; Li, B. S.; Bo, Z. S.; Lu, R. *Org. Lett.* **2004**, *6*, 4703–4706. (c) Li, B. S.; Xu, X. J.; Sun, M. H.; Fu, Y. Q.; Yu, G.; Liu, Y. Q.; Bo, Z. S. *Macromolecules* **2006**, *39*, 456–461.
(4) (a) Noh, Y. Y.; Kim, J. J.; Yoshida, Y.; Yase, K. *Adv. Mater.* **2003**, *15*, 699–702. (b) Shea, P. B.; Kanicki, J.; Pattison, L. R.; Petroff, P.; Kawano, M.; Yamada, H.; Ono, N. *J. Appl. Phys.* **2006**, *100*, 034502.
(5) Pichler, K.; Anderson, H. L.; Bradley, D. D. C.; Friend, R. H.; Hamer, P. J.; Harrison, M. G.; Jarrett, C. P.; Martin, S. J.; Stephens, J. A. *Mol. Cryst. Liq. Cryst.* **1994**, *256*, 415–422.
(6) (a) Xiao, S. Q.; Li, Y. L.; Li, Y. J.; Zhuang, J. P.; Wang, N.; Liu, H. B.; Ning, B.; Liu, Y.; Lu, F. S.; Fan, L. Z.; Yang, C. H.; Li, Y. F.; Zhu, D. B. *J. Phys. Chem. B* **2004**, *108*, 16677–16685. (b) Hagemann, O.; Jorgensen, M.; Krebs, F. C. *J. Org. Chem.* **2006**, *71*, 5546–5559. (c) Krebs, F. C.; Hagemann, O.; Jorgensen, M. *Sol. Energy Mater. Sol. Cells* **2004**, *83*, 211–228. (d) Feng, J.; Zhang, Q.; Li, W.; Li, Y.; Yang, M.; Cao, Y. *J. Appl. Polym. Sci.* **2008**, *109*, 2283–2290.
(7) (a) Eichhorn, H.; Sturm, M.; Wohrle, D. *Macromol. Chem. Phys.* **1995**, *196*, 115–131. (b) Lu, F. S.; Xiao, S. Q.; Li, Y. L.; Liu, H. B.; Li, H. M.; Zhuang, J. P.; Liu, Y.; Wang, N.; He, X. R.; Li, X. F.; Gan, L. B.; Zhu, D. B. *Macromolecules* **2004**, *37*, 7444–7450.
(8) Scamporrino, E.; Vitalini, D. *Macromolecules* **1992**, *25*, 1625–1632.
(9) Aratani, N.; Osuka, A.; Kim, Y. H.; Jeong, D. H.; Kim, D. *Angew. Chem., Int. Ed.* **2000**, *39*, 1458–1462.
(10) (a) Yamamoto, T.; Fukushima, N.; Nakajima, H.; Maruyama, T.; Yamaguchi, I. *Macromolecules* **2000**, *33*, 5988–5994. (b) Screen, T. E. O.; Lawton, K. B.; Wilson, G. S.; Dolney, N.; Ispasoiu, R.; Goodson, T.; Martin, S. J.; Bradley, D. D. C.; Anderson, H. L. *J. Mater. Chem.* **2001**, *11*, 312–320. (c) Huang, C. S.; Wang, N.; Li, Y. L.; Li, C. H.; Li, J. B.; Liu, H. B.; Zhu, D. B. *Macromolecules* **2006**, *39*, 5319–5325.
(11) (a) Laquindanum, J. G.; Katz, H. E.; Lovinger, A. J.; Dodabalapur, A. *Adv. Mater.* **1997**, *9*, 36–39. (b) Li, X. C.; Sirringhaus, H.; Garnier, F.; Holmes, A. B.; Moratti, S. C.; Feeder, N.; Clegg, W.; Teat, S. J.; Friend, R. H. *J. Am. Chem. Soc.* **1998**, *120*, 2206–2207. (c) Sirringhaus, H.; Friend, R. H.; Wang, C.; Leuninger, J.; Mullen, K. *J. Mater. Chem.* **1999**, *9*, 2095–2101. (d) Iosip, M. D.; Destri, S.; Pasini, M.; Porzio, W.; Pernstich, K. P.; Batlogg, B. *Synth. Met.* **2004**, *146*, 251–257. (e) Gao, J. H.; Li, R. J.; Li, L. Q.; Meng, Q.; Jiang, H.; Li, H. X.; Hu, W. P. *Adv. Mater.* **2007**, *19*, 3008–3011.
(12) (a) Xiao, K.; Liu, Y. Q.; Qi, T.; Zhang, W.; Wang, F.; Gao, J. H.; Qiu, W. F.; Ma, Y. Q.; Cui, G. L.; Chen, S. Y.; Zhan, X. W.; Yu, G.; Qin, J. G.; Hu, W. P.; Zhu, D. B. *J. Am. Chem. Soc.* **2005**, *127*, 13281–13286. (b) Sun, Y. M.; Ma, Y. Q.; Liu, Y. Q.; Lin, Y. Y.; Wang, Z. Y.; Wang, Y.; Di, C. A.; Xiao, K.; Chen, X. M.; Qiu, W. F.; Zhang, B.; Yu, G.; Hu, W. P.; Zhu, D. B. *Adv. Funct. Mater.* **2006**, *16*, 426–432. (c) Hunziker, C.; Zhan, X.; Losio, P. A.; Figi, H.; Kwon, O-P.; Barlow, S.; Günter, P.; Marder, S. R. *J. Mater. Chem.* **2007**, *17*, 4972–4979.
(13) Lindsey, J. S.; Prathapan, S.; Johnson, T. E.; Wagner, R. W. *Tetrahedron* **1994**, *50*, 8941–8968.
(14) Elangovan, A.; Wang, Y. H.; Ho, T. I. *Org. Lett.* **2003**, *5*, 1841–1844.
(15) Nielsen, K. T.; Spanggaard, H.; Krebs, F. C. *Macromolecules* **2005**, *38*, 1180–1189.
(16) Pommerehne, J.; Vestweber, H.; Guss, W.; Mahrt, R. F.; Bässler, H.; Porsch, M.; Daub, J. *Adv. Mater.* **1995**, *7*, 551–554.
(17) Halls, J. J. M.; Cornill, J.; dos Santos, D. A.; Silbey, R.; Hwang, D. H.; Holmes, A. B.; Brédas, J. L.; Friend, R. H. *Phys. Rev. B* **1999**, *60*, 5721–5727.
(18) Neuteboom, E. E.; Meskers, S. C. J.; Van Hal, P. A.; Van Duren, J. K. J.; Meijer, E. W.; Janssen, R. A. J.; Dupin, H.; Pourtois, G.; Cornil, J.; Lazzaroni, R.; Brédas, J. L.; Beljonne, D. *J. Am. Chem. Soc.* **2003**, *125*, 8625–8638.
(19) Li, W. R.; Kao, K. C.; Yo, Y. C.; Lai, C. K. *Helv. Chim. Acta* **1999**, *82*, 1400–1407.
(20) Lee, C. H.; Lindsey, J. S. *Tetrahedron* **1994**, *50*, 11427–11440.
(21) Pedulli, G. F.; Tiecco, M.; Guerra, M.; Martelli, G.; Zanirato, P. *J. Chem. Soc., Perkin Trans. 2* **1978**, 212–217.
(22) Zhan, X. W.; Tan, Z. A.; Domercq, B.; An, Z. S.; Zhang, X.; Barlow, S.; Li, Y. F.; Zhu, D. B.; Kippelen, B.; Marder, S. R. *J. Am. Chem. Soc.* **2007**, *129*, 7246–7247.
(23) Li, P.; Ahrens, B.; Feeder, N.; Raithby, P. R.; Teat, S. J.; Khan, M. S. *Dalton Trans.* **2005**, 874–883.

MA801407U